THE JOURNAL OF BIOLOGICAL CHEMISTRY VOL. 283, NO. 31, pp. 21621–21628, August 1, 2008

Neuronally Selective μ-Conotoxins from *Conus striatus* Utilize an α-Helical Motif to Target Mammalian Sodium Channels*[S]

Received for publication, April 14, 2008, and in revised form, May 29, 2008 Published, JBC Papers in Press, June 3, 2008, DOI 10.1074/jbc.M802852200

Christina I. Schroeder[‡1], Jenny Ekberg[§], Katherine J. Nielsen[¶], Denise Adams[‡], Marion L. Loughnan[‡], Linda Thomas[‡], David J. Adams[§], Paul F. Alewood[‡], and Richard J. Lewis[‡¶2]

From the [‡]Institute for Molecular Bioscience and the [§]School of Biomedical Sciences, The University of Queensland, Queensland 4072, Australia and [¶]Xenome Ltd, Indooroopilly, Queensland 4069, Australia

μ-Conotoxins are small peptide inhibitors of muscle and neuronal tetrodotoxin (TTX)-sensitive voltage-gated sodium channels (VGSCs). Here we report the isolation of μ-conotoxins SIIIA and SIIIB by ^{125}I-TIIIA-guided fractionation of milked *Conus striatus* venom. SIIIA and SIIIB potently displaced ^{125}I-TIIIA from native rat brain $Na_v1.2$ (IC_{50} values 10 and 5 nM, respectively) and muscle $Na_v1.4$ (IC_{50} values 60 and 3 nM, respectively) VGSCs, and both inhibited current through *Xenopus* oocyte-expressed $Na_v1.2$ and $Na_v1.4$. An alanine scan of SIIIA-(2–20), a pyroglutamate-truncated analogue with enhanced neuronal activity, revealed residues important for affinity and selectivity. Alanine replacement of the solvent-exposed Trp-12, Arg-14, His-16, Arg-18 resulted in large reductions in SIIIA-(2–20) affinity, with His-16 replacement affecting structure. In contrast, [D15A]SIIIA-(2–20) had significantly enhanced neuronal affinity (IC_{50} 0.65 nM), while the double mutant [D15A/H16R]SIIIA-(2–20) showed greatest $Na_v1.2$ *versus* 1.4 selectivity (136-fold). ^{1}H NMR studies revealed that SIIIA adopted a single conformation in solution comprising a series of turns and an α-helical motif across residues 11–16 that is not found in larger μ-conotoxins. The structure of SIIIA provides a new structural template for the development of neuronally selective inhibitors of TTX-sensitive VGSCs based on the smaller μ-conotoxin pharmacophore.

Voltage-gated sodium channels (VGSC)[3] are crucial for the excitability of nerve and muscle cells (1). Nine different VGSC isoforms ($Na_v1.1$–1.9) have been identified and characterized as either tetrodotoxin-sensitive (TTX-S) or tetrodotoxin-resistant (TTX-R) (2, 3). Of these isoforms, the TTX-R $Na_v1.8$ and 1.9 are implicated in neuropathic pain states (4, 5), the TTX-S $Na_v1.7$ is implicated in allodynia and neuropathic pain (6–10), and the TTX-S $Na_v1.3$ is up-regulated in inflammatory pain (5). To learn more about the different roles played by each of the VGSC subtypes in normal and disease states requires new inhibitors with improved VGSC subtype selectivity.

Inhibitors of TTX-S VGSCs include tetrodotoxin (TTX) from puffer fish, the saxitoxins (STXs) from marine dinoflagellates, and the μ-conotoxins from the venom of cone snails. These toxins act competitively at Site 1 in the P-loop region of the ion-conducting pore of the α-subunit of the VGSC (3, 11). While TTX and STX act with nanomolar potency across the six TTX-S VGSCs ($Na_v1.1$–1.4, 1.6, and 1.7), μ-conotoxins are more discriminating. Currently 12 μ-conotoxins have been identified from nine species of fish hunting cone snails (Table 1). μ-Conotoxins GIIIA, GIIIB, and GIIIC from *Conus geographus* selectively target the skeletal muscle $Na_v1.4$, PIIIA from *Conus purpurasence* (12–14) and TIIIA from *Conus tulipa* (15) target $Na_v1.2$ and 1.4, and μ-conotoxins SmIIIA from *Conus stercusmuscsarum* (16, 17), SIIIA from *Conus striatus* (18, 19), and KIIIA from *Conus kinoshitai* (18) target amphibian TTX-R sodium channels. More recently, KIIIA has also been shown to inhibit TTX-S sodium channels in mouse DRG and rat TTX-S sodium channels expressed in *Xenopus* oocytes (20). Lastly, μ-conotoxins CnIIIA, CnIIIB from *Conus consors*, CIIIA from *Conus catus*, and MIIIA from *Conus magus* were found to inhibit TTX-R and TTX-S sodium channels in frog DRG but not rat or mouse DRG neurons (21). Most reported μ-conotoxins have a conserved arginine in loop 2, which is essential for high affinity interactions at TTX-S sodium channels (15, 22–25). In contrast, SIIIA and KIIIA have a much shorter loop 2 and a lysine instead of an arginine in the corresponding position. Recent structure-activity studies on TIIIA (15) and KIIIA (20) have confirmed that the arginine in loop 2 is crucial for TIIIA affinity at both neuronal and skeletal muscle sodium channels, whereas the structurally equivalent lysine was only important for affinity at the skeletal muscle VGSC. Three-dimensional structures of μ-conotoxins GIIIA, GIIIB, PIIIA, TIIIA, and SmIIIA have been determined by NMR (14, 15, 17, 26, 27). These structures reveal a similar fold for the μ-conotoxins despite high sequence divergence. At present, structures of μ-conotoxins SIIIA and KIIIA are modeled from SmIIIA (18, 20, 21).

This study reports the isolation and structure-activity of μ-conotoxins SIIIA and SIIIB from the milked venom of *C. striatus.* To define aspects of their structure that contribute

* This work was supported in part by a START grant from Aus**Industry** and by National Health and Medical Research Council Project (210307) and Program (351446) Grants. The costs of publication of this article were defrayed in part by the payment of page charges. This article must therefore be hereby marked "*advertisement*" in accordance with 18 U.S.C. Section 1734 solely to indicate this fact.

[S] The on-line version of this article (available at http://www.jbc.org) contains supplemental Figs. S1 and S2.

[1] Present address: UNSW Cancer Research Centre, University of New South Wales, Sydney NSW 2052, Australia.

[2] An NHMRC Research Fellow. To whom correspondence should be addressed: Institute for Molecular Bioscience, The University of Queensland, Brisbane, Queensland 4072, Australia. Tel.: 617-3346-2984; Fax: 617-3346-2101; E-mail: r.lewis@imb.uq.edu.au.

[3] The abbreviations used are: VGSC, voltage-gated sodium channel; ACN, acetonitrile; NMR, nuclear magnetic resonance spectroscopy; RP-HPLC, reversed-phase high performance liquid chromatography; STX, saxitoxin; TTX, tetrodotoxin; RMSD, root mean-square deviation; DRG, dorsal root ganglion.

to binding to mammalian VGSCs, we determined the NMR structure of SIIIA. Distinct from other μ-conotoxins, SIIIA adopts a single conformation in solution that includes an α-helical motif not previously seen in other members of this class. This structural change was associated with a significant pharmacophore shift from the dominant arginine residue in loop 2 of the larger μ-conotoxins to a series of five similarly important residues, including four associated with the α-helical region, in the smaller SIIIA. Interestingly, a number of SIIIA analogues had significantly enhanced neuronal selectivity, opening the way to the development of subtype-selective neuronal VGSC inhibitors.

EXPERIMENTAL PROCEDURES

Isolation of μ-Conotoxins SIIIA and SIIIB—Crude *C. striatus* milked venom was separated into 80 1-min fractions by semi-preparative RP-HPLC using a Vydac C18 column (250 × 10 mm, 5 μ) eluted at 3 ml/min with a 1% gradient from 100% A to 80% B over 80 min (solvent A 0.05% trifluoroacetic acid, solvent B 90% ACN + 0.045% trifluoroacetic acid). The eluant was monitored at 230 nm and ^{125}I-TIIIA-guided fractionation (15) of the crude milked venom RP-HPLC fractions of *C. striatus* used to isolate SIIIA and SIIIB to homogeneity. The sequences of SIIIA and SIIIB (Table 1) were determined by Edman sequencing only after pyroglutamate aminopeptidase digestion, indicating that the N-terminal residue of both these conotoxins was a pyroglutamate. The observed masses for native SIIIA and SIIIB (2206.8 and 2120.7 Da, respectively) were consistent with the Edman sequencing results for peptides with an amidated C terminus. Co-injected synthetic and native SIIIA and SIIIB (2:1 ratio) co-eluted on a Vydac C18 reversed-phase HPLC column (250 × 4.6 mm, 5 μ) eluted with a 1% gradient from 100% A to 50% B over 50 min, confirming the identity of the native peptides.

Peptide Synthesis—μ-Conotoxins SIIIA and SIIIB and analogues were prepared by Boc chemistry (28) using methods described previously (14). Side-chain protecting groups chosen were Arg(Tos), Asp(OcHex), Lys(CIZ), Ser(Bzl), Asn(Xan), His(DNP), and Cys(p-MeBzl). The crude reduced peptides were purified by preparative RP-HPLC using a 1% gradient (100% A to 80% B over 80 min) and UV monitoring (230 nm), and oxidized at 0.02 mM in either aqueous 0.33 M NH_4OAc/0.5 M GnHCl/2 M NH_4OH, or 100 mM ammonium bicarbonate in the presence of oxidized and reduced glutathione (29). Oxidized peptides were purified by preparative RP-HPLC. Peptides were quantified initially by triplicate amino acid analysis to create an external reference standard for HPLC quantitation of each peptide (30). Mass spectra were acquired on a PE-Sciex API III triple quadrupole electrospray mass spectrometer in positive ion mode (m/z 500–2000 at 0.1–0.2 Da steps, declustering potentials of 10–90 V, and dwell times of 0.4–1.0 s). Data were deconvoluted using MacSpec 3.2 (Sciex, Canada) to obtain the molecular weight from the multiply charged ion species. Mass spectrometry was used to confirm purity and to monitor peptide oxidation (data not shown).

Chemicals and Reagents—Acetonitrile, methanol, ethanol, and glacial acetic acid were from BDH (Poole, UK). Phenyl isothiocyanate and amino acid standards were from Pierce. HBTU, dimethyl formamide, dichloromethane, trifluoroacetic acid, *N*,*N*-diisopropylethylamine, dicyclohexylcarbodiimide, and 1-hydroxybenzotriazole were all peptide synthesis grade from Auspep (Melbourne, Australia). *p*-Methylbenzhydrylamine 1% cross-linked divinylbenzene polystyrene resin was from the Peptide Institute (Osaka, Japan), and BocPAM-Phe resin was from Applied Biosystems (Fosters City, CA). Purified water was obtained from a tandem Milli-RO/Milli-Q system (Bedford, MA). *p*-Cresol, *p*-thiocresol, guanidine·HCl (99%+), reduced and oxidized glutathione, and triethylamine (freshly distilled) were from Sigma Aldrich. Anhydrous hydrogen fluoride (HF) was supplied by BOC Gases (Brisbane, Australia). Ammonium acetate (AR) and ammonium sulfate (AR) was from Ajax Chemicals (Australia). Boc-L-amino acids were purchased from Bachem and Novabiochem (La Jolla, CA). All other reagents and solvents were ACS analytical reagent grade.

Radioligand Binding Studies—^{125}I-TIIIA (prepared using IODOGEN) radioligand binding studies were performed using rat brain and rat skeletal muscle preparations to measure $Na_v1.2$ and $Na_v1.4$ affinity, as previously described (15). Nonlinear regressions (Hillslope-1) were fitted to triplicate data obtained for each experiment using Prism software (GraphPad, San Diego, CA).

Recording of Depolarization-activated Sodium Ion Currents in Rat DRG Neurons—Neonatal rat DRG neurons were prepared as described previously (31). Whole cell TTX-S and TTX-R sodium ion currents were recorded in using an Axopatch 200A patch clamp amplifier (Molecular Devices Corp.). Series resistance was routinely compensated by 70–80%. Capacitive and leakage currents were digitally subtracted using a −P/6 pulse protocol. Internal pipette solution contained (in mM): NaCl 10, CsF 130, CsCl 10, EGTA 10, HEPES-CsOH 10, pH 7.2, 290–300 mOsM (with sucrose). The bath solution contained (in mM): NaCl 50, KCl 5, $MgCl_2$ 1, $CaCl_2$ 1, glucose 10, tetraethylammonium (TEA)-Cl 90, HEPES-TEA-OH 10, pH 7.35. TTX-resistant sodium ion currents were recorded from small DRG neurons (≤25 μm diameter) in the presence of 300 nM TTX. Large neurons (≥40 μm diameter), in which the sodium ion current exhibited fast activation and inactivation kinetics and was mostly TTX-sensitive (>90%), were used to study toxin effects on TTX-S sodium ion current after complete washout of TTX block. Toxins were diluted in extracellular solution and added via a gravity-fed perfusion system.

Xenopus Oocyte Experiments—Depolarization-activated sodium ion currents were recorded from *Xenopus* oocytes expressing various VGSC α-subunit subtypes using a two-electrode (virtual ground circuit) voltage clamp at room temperature (20–23 °C) with a GeneClamp 500B amplifier and pCLAMP 8 software (Axon Instruments Inc, Union City, CA). Bath solution contained (in mM) 100 NaCl, 2 KCl, 1 $MgCl_2$, 0.3 $CaCl_2$, and 20 HEPES-NaOH, pH 7.5. Data were low pass-filtered at 2 kHz, digitized at 10 kHz, and leak-subtracted on-line using a −P/6 protocol and analyzed off-line. Data were analyzed using Clampfit 8 software (Axon Instruments Inc., Union City, CA). Rat $Na_v1.2$ and rat $Na_v1.3$ was a gift from A. Goldin (University of California), human $Na_v1.5$ a gift from R. Kass (Columbia University), and human $Na_v1.7$ a gift from N. Klugbauer (Teknischen Universität, Munich). Toxins were added by

direct bath application (static bath) followed by extensive mixing to reach the final concentrations stated. The steady-state block was reached after ~8 min of toxin exposure, and washout of SIIIA was followed for 20–30 min.

^{1}H Nuclear Magnetic Resonance (NMR) Spectroscopy—All NMR experiments were recorded on a Bruker ARX 500 spectrometer equipped with a *z*-gradient unit, a Bruker DMX 750, or a Bruker 600 Avance spectrometer equipped with a *x,y,z*-gradient unit. Peptide concentrations were ~2 mM. SIIIA and SIIIB were examined in 95% H_2O/5% D_2O (pH 3.0, 275–298 K) and in 100% D_2O (260–293 K). SIIIA analogues were examined in 90% H_2O/10% D_2O, pH 3.0. For SIIIA, ^{1}H NMR experiments recorded included NOESY, (mixing times 120, 300, and 400 ms), TOCSY (mixing time 80 ms), double-quantum filtered (DQF)-COSY, and E-COSY in 100% D_2O. Slowly exchanging amide protons were detected by acquiring one-dimensional NMR spectra immediately after dissolving the peptide in 100% D_2O at pH 3.5. For all other analogues, TOCSY experiments with a mixing time of 80 ms were acquired. Additional NOESY experiments were only run if ambiguities arose during assignment. All spectra were run over 6024 Hz (500 MHz), 7184 Hz (600 MHz), or 8192 Hz (750 MHz) with 4K data points, 400–512 FIDs, 8–64 scans, and a recycle delay of 1–2 s. The solvent was suppressed using the WATERGATE sequence (32). Spectra were processed using UXNMR as described previously (29) and using Aurelia, subtraction of background was used to minimize T_1-noise. Chemical shift values of SIIIA and analogues were obtained in 90% H_2O, 10% D_2O and referenced internally to DSS at 0.00 ppm. Secondary Hα shifts were measured and compared with values for random coil shifts (33).

SIIIA was assigned in sparky (34), and distance information obtained by integration of a 300 ms mixing time NOESY spectrum. Backbone dihedral restraints were derived from $^3J_{HN\text{-}H\alpha}$ coupling constants from a DQF-COSY spectrum or a one-dimensional ^{1}H NMR spectrum. The ϕ dihedral angle restraints included were restrained to 120 ± 30° for $^3J_{HN\text{-}H\alpha} > 8$ Hz and −60 ± 30° for $^3J_{HN\text{-}H\alpha} < 5.8$ Hz. χ1 dihedral angels were determined from intraresidue nuclear Overhauser effect (NOE) and $^3J_{H\alpha\text{-}H\beta}$ coupling patterns for an E-COSY spectrum. Initial structures were generated using dyana (35), and final structures were calculated in explicit water with CNS (36) as previously described (37). An initial 50 structures were calculated, and the 17 lowest overall energy structures selected to represent the solution structure of SIIIA.

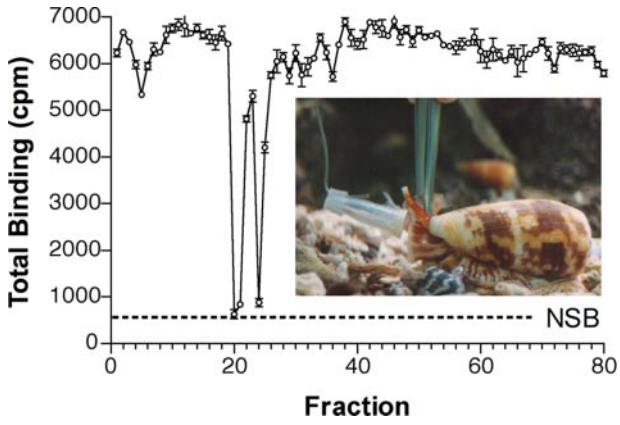

FIGURE 1. **Identification of native SIIIA and SIIIB in milked crude *C. striatus* venom.** Active fractions eluting from RP-HPLC using a 1% gradient (0–80% B solvent B: 90% ACN, 0.045% trifluoroacetic acid) displaced ^{125}I-TIIIA-(2–22) binding to rat brain. *Dashed line* indicates non-specific binding, and *inset* shows *Conus striatus* venom being collected by milking.

RESULTS

Isolation of μ-Conotoxins SIIIA and SIIIB—To identify μ-conotoxins selective for neuronal VGSCs, fractionated milked *C. striatus* venom was assayed for the ability to displace ^{125}I-TIIIA from rat brain sodium channels (15). Three active fractions with retention times of 20, 21, and 24 min (Fig. 1) were purified to homogeneity, digested using pyroglutaminase, and Edman-sequenced to reveal three peptides with a CC-C-C-CC motif characteristic of μ-conotoxins (38). Fraction 24 contained the sequence of TIIIA, previously identified in *C. tulipa* by PCR (15), fraction 20 the sequence for SIIIA, while fraction 21 contained a sequence for a new μ-conotoxin we named SIIIB (Table 1). SIIIA and SIIIB each comprised 20 residues with a net charge of +2 and +3, respectively. Mass spectrometry and co-elution studies of the native and synthetic peptides confirmed the sequences and C-terminal amidation of both peptides (data not shown).

Radioligand Binding Studies—Synthetic μ-conotoxin SIIIA and SIIIB each potently displaced ^{125}I-TIIIA from VGSCs in rat brain and rat skeletal muscle (Fig. 2). The pIC_{50} values for SIIIA and SIIIB and selected additional μ-conotoxins are summarized in Table 2. Similar to TTX and STX, SIIIA had a small but

TABLE 1

μ-Conotoxin sequences and VGSC selectivity

Z, Pyroglutamate; O, hydroxyproline.

Peptide[a]	Sequence	Selectivity	Ref.
SIIIB	ZN–**CC**NG--G**C**SSKW**C**KGHAR**CC**[b]	1.4 ≈ 1.2	This work
SIIIA	ZN–**CC**NG--G**C**SSKW**C**RDHAR**CC**[b]	1.2 ≈ 1.4	This work (18, 19)
KIIIA	---**CC**N----**C**SSKW**C**RDHSR**CC**[b]	1.2 ≈ 1.4	(18, 20)
SmIIIA	ZR–**CC**NGRRG**C**SSRW**C**RDHSR**CC**[b]	Amphibian	(16)
MIIIA	Z–G**CC**NVPNG**C**SGRW**C**RDHAQ**CC**[b]	Amphibian	(21)
CIIIA	-GR**CC**EGPNG**C**SSRW**C**KDHAR**CC**[b]	Amphibian	(21)
CnIIIA	-GR**CC**DVPNA**C**S-RW**C**RDHAQ**CC**[b]	Amphibian	(21)
CnIIIB	Z–G**CC**GEPNL**C**FTRW**C**RNNAR**CC**RQQ[c]	Amphibian	(21)
TIIIA	RHG**CC**KGOKG**C**SSRE**C**RO-QH**CC**[b]	1.4 ≈ 1.2	(15)
PIIIA	ZRL**CC**GFOKS**C**RSRQ**C**KO-HR**CC**[b]	1.4 ≈ 1.2	(24)
GIIIA	RD-**CC**TOOKK**C**KDRQ**C**KO-QR**CC**A[b]	1.4 ≫1.2	(38)
GIIIB	RD-**CC**TOORK**C**KDRR**C**KO-MK**CC**A[b]	1.4 > 1.2	(38)
GIIIC	RD-**CC**TOOKK**C**KDRR**C**KO-LK**CC**A[b]	1.4 ≫ 1.2	(38)

[a] SIIIA, SIIIB, and KIIIA are smaller μ-conotoxins, whereas the others are defined as larger μ-conotoxins.
[b] C-terminal amidation.
[c] Free acid C-terminal. Cysteines 1–4, 2–5, 3–6 are paired.

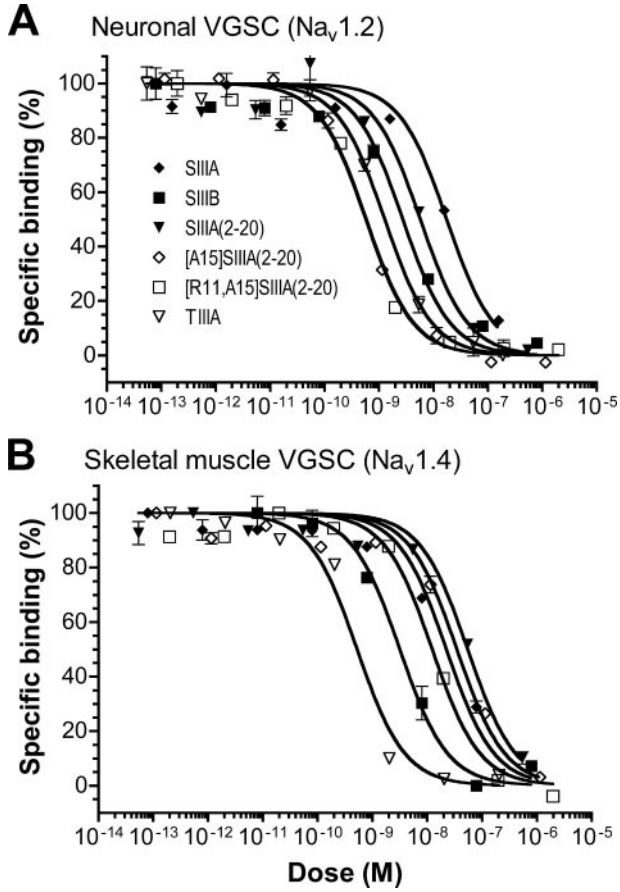

FIGURE 2. Displacement of ^{125}I-TIIIA from (*A*) rat brain $Na_v1.2$ and (*B*) rat skeletal muscle $Na_v1.4$ VGSCs by SIIIA (◆), SIIIB (■), and selected SIIIA analogues, SIIIA-(2–20) (▼) [D15A]SIIIA-(2–20) (◇), and [R11,A15]SIIIA-(2–20) (□), as well as TIIIA for comparison (▽).

TABLE 2

μ-Conotoxin affinity (pIC_{50} ± S.E.) determined from displacement of ^{125}I-TIIIA from rat brain and skeletal muscle sodium channels ($n = \geq 3$)

μ-Conotoxin	Brain ($Na_v1.2$)	Muscle ($Na_v1.4$)	Selectivity[a]
SIIIA	8.02 ± 0.12	7.67 ± 0.13	0.35
SIIIB	8.29 ± 0.15	8.49 ± 0.11	−0.20
TIIIA	9.27 ± 0.06	9.72 ± 0.08	−0.45
PIIIA	8.72 ± 0.07	9.05 ± 0.05	−0.33
GIIIA	6.47 ± 0.27	10.0 ± 0.05	−3.53
GIIIB	7.85 ± 0.15	10.0 ± 0.05	−2.15
GIIIC	6.34 ± 0.16	10.0 ± 0.05	−3.62
STX	9.35 ± 0.05	8.90 ± 0.06	0.45
TTX	8.16 ± 0.21	7.32 ± 0.18	0.84

[a] Neuronal selectivity calculated as brain pIC_{50} − muscle pIC_{50}.

significant preference for neuronal $Na_v1.2$ over the skeletal muscle $Na_v1.4$, whereas SIIIB had a preference for $Na_v1.4$. Both SIIIA and SIIIB were full inhibitors of ^{125}I-TIIIA binding to rat brain or skeletal muscle sodium channels. Interestingly, removing the pyroglutamate residue at the N terminus (SIIIA-(2–20) and SIIIB-(2–20)) enhanced SIIIA and decreased SIIIB activity at $Na_v1.2$, while the reverse effect was observed at $Na_v1.4$ (Fig. 4). These shifts in potency made SIIIA-(2–20) more $Na_v1.2$-selective and SIIIB-(2–20) more $Na_v1.4$-selective. Like TIIIA, SIIIA was unable to fully displace [^{3}H]STX from rat brain (data not shown) suggesting selectivity for $Na_v1.2$ over other TTX-S sodium channels. All displacement curves were best fitted with a Hill slope of −1.

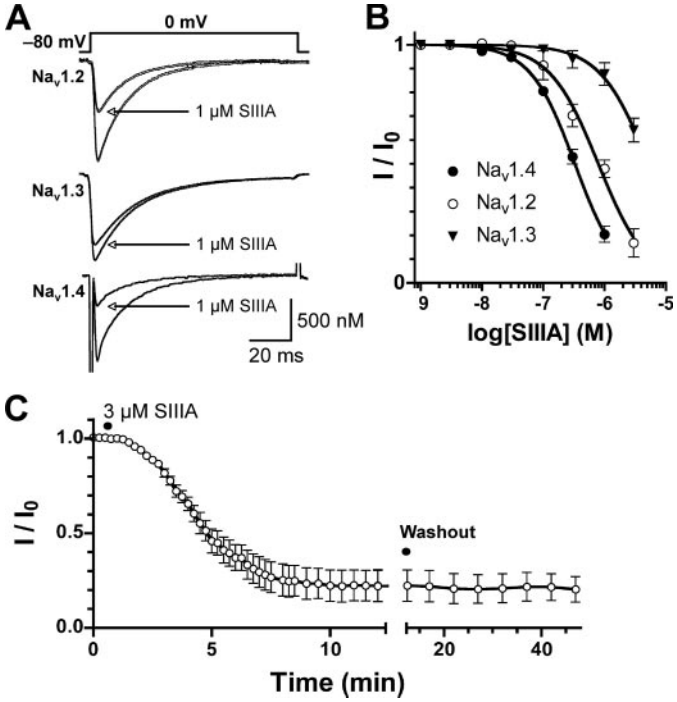

FIGURE 3. **Inhibition of recombinant VGSCs expressed in *Xenopus* oocytes by μ-conotoxin SIIIA.** *A*, superimposed depolarization-activated sodium ion currents mediated by $Na_v1.2$, $Na_v1.3$, and $Na_v1.4$ in the absence and presence of 1 μM SIIIA. Oocytes were held at −80 mV and depolarized to 0 mV every 5 s. *B*, concentration-response curves obtained for SIIIA inhibition of $Na_v1.2$, $Na_v1.3$, and $Na_v1.4$ (n = 3–5). *C*, kinetics of SIIIA inhibition of $Na_v1.2$. The on-rate curve was fitted with a single exponential function, yielding a τ_{on} of 4.0 min for 3 μM SIIIA. Inhibition was not reversed upon washout for up to 30 min ($n = 3 \pm$ S.E.).

Effects of SIIIA on Whole Cell Sodium Ion Currents—The effects of μ-conotoxin SIIIA was investigated on both TTX-S and TTX-R sodium ion current in neonatal rat DRG (31). SIIIA at 3 μM produced no detectable inhibition of either TTX-S or TTX-R sodium ion currents in rat DRG neurons (data not shown).

Effects of μ-Conotoxins on Oocyte-expressed VGSC Subtypes—SIIIA was examined for inhibition of sodium ion current through VGSC subtypes expressed in *Xenopus* oocytes. SIIIA at 3 μM caused 95% inhibition of $Na_v1.2$ current, 45% inhibition of $Na_v1.3$ current (Fig. 3*A*), but no detectable inhibition of sodium ion current through $Na_v1.5$, $Na_v1.7$, or $Na_v1.8$ (data not shown). The IC_{50} values for SIIIA was 790 nM (95% CI 630–990 nM) at $Na_v1.2$, 330 nM (95% CI 300–360 nM) at $Na_v1.4$, and 5.3 μM (95% CI 3.6–7.6 μM) at $Na_v1.3$ (Fig. 3*B*). SIIIB at 3 μM caused 93% inhibition of $Na_v1.2$ current and 10% inhibition of $Na_v1.7$ current (data not shown) but was not tested on other VGSC subtypes. The inhibitory effect of SIIIA was not reversed upon washout (Fig. 3*C*), in contrast to TIIIA which was fully reversible upon washout at $Na_v1.2$ (15).

Affinity of μ-Conotoxin Analogues—The affinity of μ-conotoxin analogues of SIIIA and SIIIB are shown in Fig. 4. SIIIA-(2–20) had decreased affinity at $Na_v1.4$, but increased binding affinity at $Na_v1.2$ sodium channel, whereas SIIIB-(2–20) had increased affinity at both subtypes. In an attempt to identify residues contributing to the neuronal selectivity, we produced an alanine scan of SIIIA-(2–20), except for the small Asn, Gly, and Ser residues in loops 1 and 2. Surprisingly, [K11A]SIIIA-

(2–20) had only a small 6-fold reduction in affinity at $Na_v1.2$ and $Na_v1.4$, compared with the ~100–300-fold reduction in affinity for the equivalent substitution in TIIIA ([R14A]TIIIA at rat $Na_v1.2$) (15) and GIIIA ([R13A]GIIIA at rat $Na_v1.4$) (39). In contrast, the adjacent mutant [W12A]SIIIA-(2–20) had 22- and 87-fold reduced affinity compared with SIIIA-(2–20) at $Na_v1.2$ and $Na_v1.4$, respectively, similar to that reported for KIIIA (20). Removing the negative charge at position 15 in [D15A]SIIIA-(2–20) produced a 10-fold increased affinity at $Na_v1.2$ without affecting $Na_v1.4$ affinity, resulting in 70-fold neuronal selectivity. This enhanced affinity was lost if Asp-15 was replaced with a positive charge (*e.g.* lysine) or an aromatic residue (*e.g.* tyrosine). The double mutant [K11R/D15A]SIIIA-(2–20) had a similar potency and slightly enhanced $Na_v1.2$ selectivity compared with [D15A]SIIIA-(2–20), indicating that the lysine in loop 2 of SIIIA can be interchanged with arginine without loss of affinity.

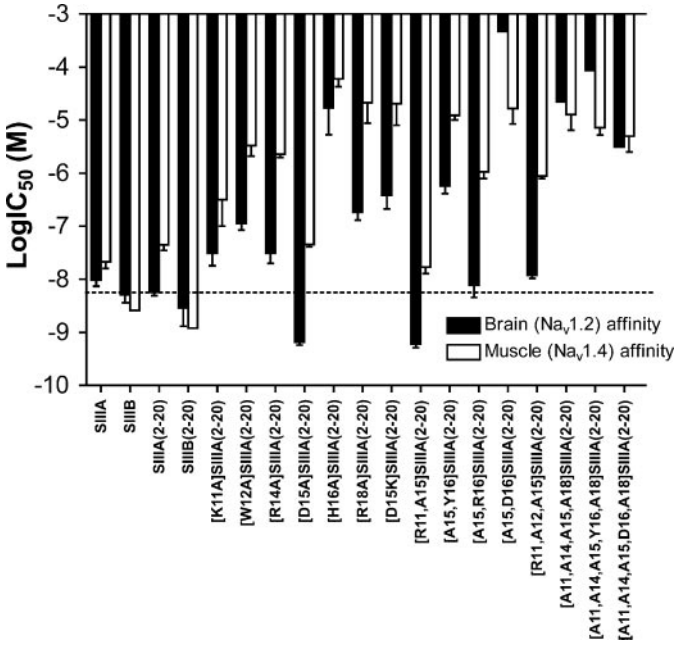

FIGURE 4. **Affinity and selectivity of SIIIA, SIIIB and analogues at rat brain ($Na_v1.2$) and rat skeletal muscle ($Na_v1.4$) VGSCs.** The IC_{50} values to displace ^{125}I-TIIIA at rat brain and skeletal muscle membrane (mean ± S.E.) are shown. The *dotted line* indicates SIIIA-(2–20) neuronal affinity. n = 2–10 experiments each performed in triplicate, except those without error bars, which were obtained from a single experiment.

Of the mutants tested, [H16A]SIIIA-(2–20) showed the largest drop in affinity at both $Na_v1.2$ and $Na_v1.4$, confirming the results reported for KIIIA (20). Interestingly, the double mutant [D15A/H16R]SIIIA-(2–20) where the negative charge from Asp was removed and an adjacent positive charge was introduced, had similar affinity at $Na_v1.2$ but a 30-fold loss of affinity at $Na_v1.4$ compared with SIIIA-(2–20), making it the most neuronally selective μ-conotoxin identified in this study (137-fold selective). In contrast, the corresponding Asp-16 analogue [D15A/H16D]SIIIA-(2–20) had dramatically (100,000-fold) reduced affinity at $Na_v1.2$ and 400-fold reduced affinity at $Na_v1.4$, compared with native SIIIA-(2–20), producing a $Na_v1.4$-selective peptide. The C-terminal arginine analogue [R18A]SIIIA-(2–20) had ~ 30-fold reduced affinity for $Na_v1.2$ compared with SIIIA(2–20) and ~ 500-fold reduced affinity for $Na_v1.4$ to yield a second neuronally (116-fold) selective peptide. As anticipated, [A11,A14,A15,D16,A18]SIIIA-(2–20), [A11,A14,A15,Y16,A18]SIIIA-(2–20), and [A11,A14,A15,A18]SIIIA-(2–20) had significantly reduced affinity compared with SIIIA-(2–20), particularly at $Na_v1.2$.

To identify the structural determinants underlying these shifts in affinity and selectivity, the three-dimensional solution structure of SIIIA was calculated using ^{1}H NMR spectroscopy. In addition, Hα chemical shifts were determined to establish that each analogue adopted the native fold found in SIIIA.

^{1}H NMR Spectroscopy—Apart from TIIIA, spectral assignment and structure calculations have proved difficult for μ-conotoxins due to Pro/Hyp *cis/trans* isomerization that produces line-broadening and multiple conformations (14, 26, 27). Consistent with the absence of Pro/Hyp residues in SIIIA, NMR data indicated that a single conformation for SIIIA and analogues dominated in solution. Only [H16A]SIIIA-(2–20) showed a significant change in backbone Hα-chemical shift, indicating that His-16 provides structural stabilization, especially to the C-terminal-half of the peptide (Fig. 5). Interestingly, [A15,R16]SIIIA-(2–20) and [A11,A14,A15,Y16,A18]SIIIA-(2–20) did not show a change in secondary Hα-chemical shifts, apart from minor local shifts at residue 15 or 11, respectively, suggesting that arginine and tyrosine (but not Ala) can replace His-16 as a structural stabilizer. The three-dimensional SIIIA structure is described below.

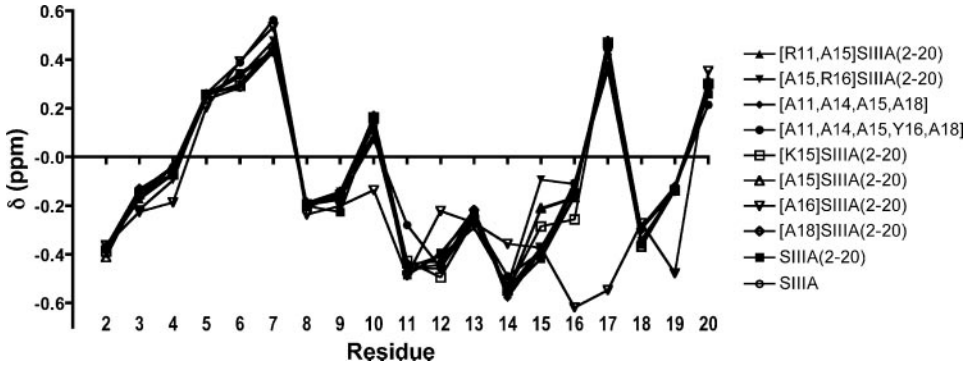

FIGURE 5. **Secondary Hα shifts (δ, ppm) for SIIIA, SIIIA-(2–20) and selected SIIIA-(2–20) analogues.** A significant change in backbone structure was seen for [A16]SIIIA-(2–20), while the [A11,A14,A15,Y16,A18]SIIIA-(2–20) and [A11,A14,A15,A18]SIIIA-(2–20) analogues had secondary Hα shifts similar to native SIIIA and SIIIA-(2–20).

SIIIA was examined by NMR spectroscopy under aqueous conditions over a range of different temperatures to confirm proton assignments (data not shown). NMR solution structures were then calculated based on a total of 288 distance restraints derived from 102 intra-residue, 93 sequential, 89 medium- and long-range NOEs, 4 hydrogen bond restraints defining 2 hydrogen bonds, and 12 ϕ and one χ1 dihedral angle restraints. A total of 46 of 50 structures converged to a consensus structure. These structures con-

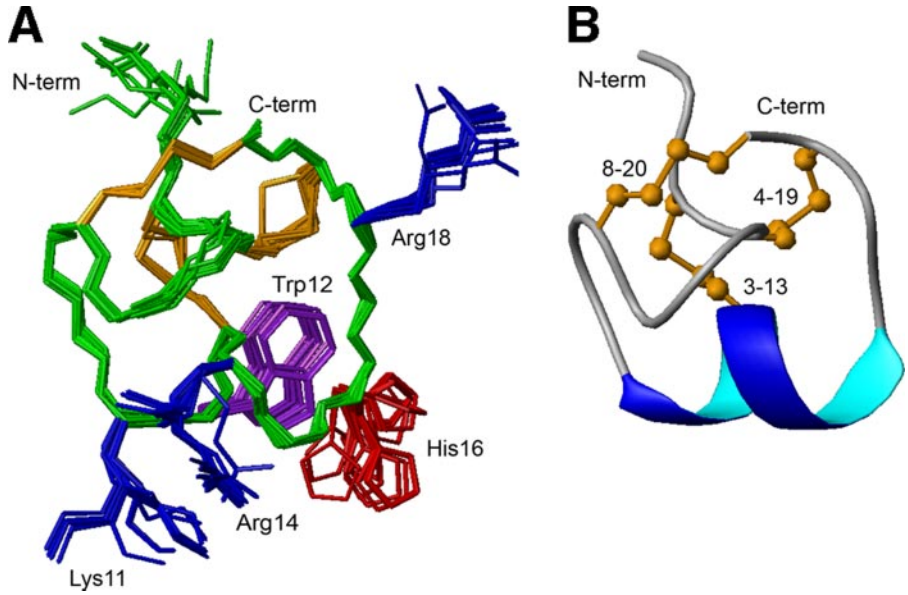

FIGURE 6. **Three-dimensional NMR structure of SIIIA.** *A*, SIIIA backbone superimposed over region 3–20 for the 17 lowest energy structures. Shown are Lys-11, Arg-14, and Arg-18 (*blue*), Trp-12 (*purple*), and His-16 (*red*), which influenced affinity at VGSCs. *B*, *ribbon representation* of the average structure of SIIIA showing the α-helical motif across residues 11–16. Disulfide bonds are shown in *orange*.

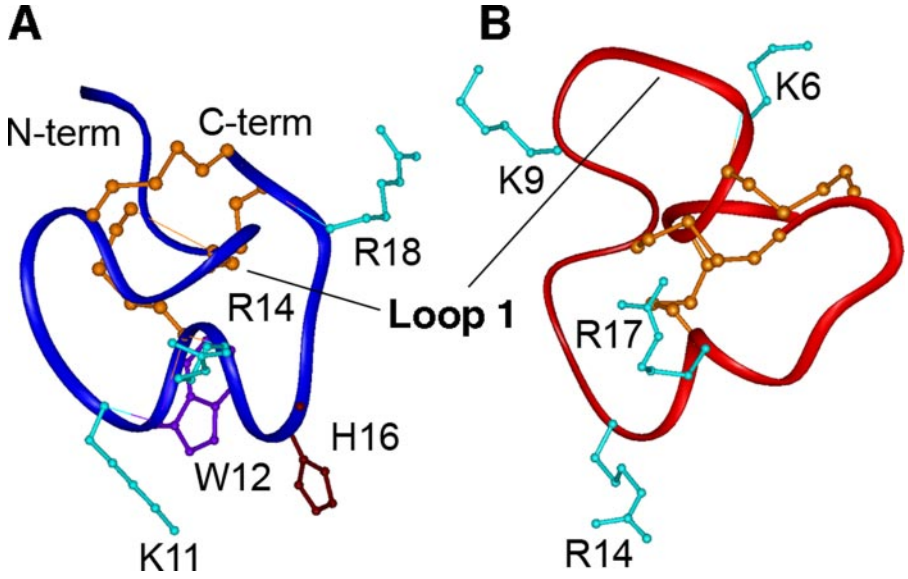

FIGURE 7. **Comparison of μ-conotoxin SIIIA and TIIIA NMR structures.** Representative *ribbon structures* of (*A*) SIIIA and (*B*) TIIIA (15), superimposed across residues 8–13 (SIIIA) and 11–16 (TIIIA) to highlight the different orientations of loop 1. Residues influencing VGSC affinity are indicated. Arg-14 is critical for high affinity interactions of TIIIA, and other larger μ-conotoxins (see supplemental Fig. S2), while Lys-11, Trp-12, Arg-14, and Arg-18 contribute similarly to SIIIA affinity. His-16 in SIIIA appeared to affect VGSC affinity by perturbing backbone structure. Disulfide bonds are shown in *orange*. See BMRB accession codes 20024 (TIIIA) and 20025 (SIIIA).

tained 2 NOE violations greater than 0.2 Å and no dihedral violations greater than 3°. The local and medium range NMR data that provide information on the secondary structure of SIIIA are given in supplemental Fig. S1*A*. The presence of several Hα-NH_{i+2}, NH-NH_{i+2}, Hα-NH_{i+3}, and Hα-NH_{i+3} NOEs suggested the presence of several turns, and identified that a helical secondary structure existed across residues 11–16. This α-helical motif was supported by a number of *i-i+3* and *i-i+4* NOEs and the presence of small $^3J_{HN\text{-}H\alpha}$ dihedral angles and negative secondary Hα-chemical shifts in this region of the peptide (Fig. 5).

The 17 lowest energy structures of SIIIA are superimposed globally in Fig. 6*A*, and a representative ribbon structure highlighting secondary structural motifs is shown in Fig. 6*B*. Overall, the structures are well-defined with a backbone root mean-square deviation (RMSD) of 0.21 across residues 3–20 and 0.35 across residue 1–20. The angular order parameters for ϕ and ψ angles are also well ordered and >0.92 across residues 6–20. The slightly disordered N-terminal residues do not appear to arise from conformational exchange or structural flexibility, because no line-broadening was observed for these residues, and are more likely due to a lack of NOEs to loop 1, which contains two Gly residues. Unlike the longer loop 1 in other μ-conotoxins, which protrudes outward, loop 1 of SIIIA comprises a tightly folded β-turn-like motif that is positioned to interact with loop 3 (see Fig. 7). Analysis of the surface exposure of each residue illustrates this structural shift, with loop 1 and the first two residues in loop 2 of SIIIA being relatively buried compared with the equivalent region of TIIIA (15), whereas Lys-11, Trp-12, Arg-14 within the α-helical region, together with Arg-18, are relatively exposed to solvent (supplemental Fig. S1*B*). As expected, all Cys residues are buried in the core of the molecule. Comparing the NMR structures of SIIIA and TIIIA reveals that the key binding determinants of SIIIA are distributed across the α-helical motif (Lys-11, Trp-12, Arg-14), and Arg-18 with each contributing similarly to affinity, whereas a single arginine (Arg-14) is the key determinant of TIIIA affinity (Fig. 7). In supplemental Fig. S2, these comparisons are extended to PIIIA, GIIIA, and SmIIIA.

DISCUSSION

The venoms of cone snails provide a rich source of μ-conotoxin inhibitors of VGSCs, including several recently isolated μ-conotoxins with a smaller loop 2 (18, 19). In this study we used assay-directed fractionation of milked *C. striatus* venom to identify a new μ-conotoxin SIIIB, together with the recently reported SIIIA (18) and TIIIA (15). Interestingly, the smaller μ-conotoxins from *C. striatus* exploit a new pharmacophore

that allows the development of peptides with selectivity for $Na_v1.2$ and potentially other TTX-S subtypes.

SIIIA and SIIIB both displaced ^{125}I-TIIIA and [^{3}H]STX binding to rat brain ($Na_v1.2$) and rat skeletal muscle membrane ($Na_v1.4$), indicating they act at site 1 of the VGSC like the larger μ-conotoxins PIIIA (24), TIIIA (15), GIIIA, and GIIIB (38). SIIIA also inhibited current through oocyte-expressed $Na_v1.2$ and $Na_v1.4$ at nanomolar potencies, confirming it acts as a pore blocker of mammalian VGSCs. Like KIIIA (20), inhibition of $Na_v1.2$ was not reversed by toxin washout. SIIIA also inhibited current through $Na_v1.3$ at higher concentrations, showing that these smaller μ-conotoxins have the potential to target additional neuronal subtypes. μ-Conotoxins SIIIA, KIIIA, SmIIIA, CnIIIA, and CIIIA all potently inhibit frog TTX-R sodium ion current (18, 21). However, we were unable to detect any inhibition of TTX-R or TTX-S sodium ion current in rat DRG neurons by SIIIA, in contrast to an earlier study showing inhibition of the TTX-R current in adult rat DRG by SIIIA (19). The inability of SIIIA to inhibit TTX-S sodium ion current in neonatal rat DRG indicates that $Na_v1.2$ and 1.3 are not expressed at significant levels in these neurons.

A number of analogues of SIIIA and SIIIB, and the neuronally selective truncated SIIIA-(2–20), were synthesized to identify residues contributing to VGSC affinity and selectivity. A loop 2 lysine is present in SIIIA and SIIIB instead of the corresponding arginine previously found to be critical for high affinity interactions of the larger μ-conotoxins GIIIA (39–41), PIIIA (24), SmIIIA (17), and TIIIA (15). However, the [K11A]SIIIA-(2–20) analogue revealed that this loop 2 lysine contributes only modestly to VGSC affinity, producing a 6-fold reduction in affinity for $Na_v1.2$ or $Na_v1.4$ compared with SIIIA-(2–20). Additional SIIIA analogues [W12A]SIIIA-(2–20), [K14A]SIIIA-(2–20), and [R18A]SIIIA-(2–20) revealed that Trp-12, Lys-14, and Lys-18 also contribute significantly to affinity at $Na_v1.4$ and to a lesser extent $Na_v1.2$ affinity. The single mutant [D15A]SIIIA-(2–20) had enhanced affinity for $Na_v1.2$ and unchanged $Na_v1.4$ affinity, making it one of the most selective SIIIA analogues identified. However, other substitutions (*e.g.* Tyr-15 or Lys-15) were not well tolerated, showing that a small hydrophobic side chain is preferred at position 15 in SIIIA. An alanine scan of KIIIA revealed that the corresponding Trp-8, Arg-10, and Arg-14 also contributed to $Na_v1.2$ affinity, with Lys-7 and Asp-11 contributing only to $Na_v1.4$ affinity (20). Thus, the pharmacophore for the smaller μ-conotoxins SIIIA and KIIIA are similar, with residues important for the high affinity of SIIIA at VGSCs located along the α-helical motif plus Arg-18 (Fig. 6). In comparison, the pharmacophore of larger μ-conotoxins including TIIIA is dominated by an arginine in loop 2 (Fig. 7 and supplemental Fig. S2).

Replacing His-16 with alanine also had a dramatic effect on SIIIA and KIIIA (20) affinity. However, Hα-chemical shift changes indicated that this altered affinity arises, at least in part, from changes in structure of the C-terminal half of the peptide that potentially disrupt the α-helix and thus the orientations of the major binding determinants required for high affinity interactions at VGSCs. Interestingly, the potent and $Na_v1.2$-selective [D15A/H16R]SIIIA-(2–20) did not show a change in secondary Hα-chemical shifts, apart from minor local shifts at residue 15, indicating that Arg-16 might play a similar structural role to His-16.

Comparing the NMR solution structure of SIIIA with TIIIA it is apparent they adopt distinct conformations in solution (Fig. 7). Superimposition of loop 2 residues 8–13 of SIIIA with the corresponding residues 11–16 of TIIIA and PIIIA and gave high RMSDs of 1.08 1.53, respectively. This affect is even more dramatic when SIIIA and SmIIIA are compared across loops 2 and 3 (RMSD of 2.58), despite having almost identical sequences. In contrast, comparing the same residues between PIIIA and TIIIA gave a lower RMSD of 0.64. Examining the secondary structures of the different μ-conotoxins provides an explanation. GIIIA, GIIIB, PIIIA, SmIIIA, and TIIIA each comprise a series of turns and loops (14, 15, 17, 25, 27, 42), with a β-hairpin seen in the N-terminal part of GIIIA and GIIIB and the minor conformation of PIIIA (14). These turns in GIIIB, SmIIIA, PIIIA, and TIIIA produce a 3^{10}-helix across residues 13–22, 13–20, 13–17, and 12–15, respectively (numbering specific to each conotoxin) (14, 15, 17, 25, 27, 42) compared with the α-helix found in SIIIA. Previously described structures of SIIIA and KIIIA (18, 20, 21), as well as CnIIIA, CnIIIB, CIIIA, and MIIIA (21), were modeled from the NMR structure of SmIIIA (17). However, the NMR solution structures of SIIIA reveals that loop 1 of SIIIA is not extended as seen in TIIIA (Fig. 7) and other larger μ-conotoxins (supplemental Fig. S2) but instead folds in toward the α-helical region. This altered conformation, supported by a series of long-range NOEs between loops 1 and 3, within loops 2 and 3, and between loops 2 and 3, permits a more extended C-terminal region not seen in the larger μ-conotoxins. Interestingly, these structural shifts allow Lys-11, Arg-14, and Arg-18 of SIIIA and Arg-14, Arg-17, and Lys-6 of TIIIA to adopt similar relative positions (Fig. 7) that might allow binding to a negatively charged crevice in or near the mouth of the VGSC. A comparison of the sequences of KIIIA, SIIIA, and SIIIB reveals they are similar across loops 2 and 3, and include all important binding determinants, suggesting they likely have similar binding modes and similar conformations in solution.

The present study of SIIIA and SIIIB extends our knowledge of the structure-activity relationship of smaller μ-conotoxins and defines key residues contributing to $Na_v1.2$ selectivity. SIIIA contains an α-helix across residues 11–16 unlike previously determined μ-conotoxin NMR structures. The reduction in size of loop 1 from five residues in the larger μ-conotoxins to three in smaller μ-conotoxins like SIIIA appears to underlie a shift from a 3^{10}-helical motif to the α-helix. SIIIA targets $Na_v1.2$, 1.3, and 1.4, whereas the even smaller KIIIA additionally targets $Na_v1.1$, 1.6, and 1.7 (20), indicating that the size of loop 1 can influence not only the structure but also the selectivity of μ-conotoxins. The range of VGSC subtypes inhibited by these smaller μ-conotoxins opens the door to the development of peptides with novel subtype specificity and analgesic potential.

Acknowledgment—We thank Alun Jones who assisted with the MS analyses.

REFERENCES

1. Catterall, W. A. (2000) *Neuron* **26,** 13–25
2. French, R. J., and Terlau, H. (2004) *Curr. Med. Chem.* **11,** 3053–3064
3. Catterall, W. A., Goldin, A. L., and Waxman, S. G. (2005) *Pharmacol. Rev.* **57,** 397–409
4. Kalso, E. (2005) *Curr. Pharm. Des.* **11,** 3005–3011
5. Wood, J. N., Boorman, J. P., Okuse, K., and Baker, M. D. (2004) *J. Neurobiol.* **61,** 55–71
6. Luy, Y. S., Park, S. K., Chung, K., and Chung, J. M. (2000) *Brain Res.* **871,** 98–103
7. Boucher, T. J., Okuse, K., Bennett, D. L., Munson, J. B., and Wood, J. N. (2000) *Science* **290,** 124–127
8. Nassar, M. A., Stirling, L. C., Forlani, G., Baker, M. D., Matthews, E. A., Dickenson, A. H., and Wood, J. N. (2004) *Proc. Natl. Acad. Sci. U. S. A.* **101,** 12706–12711
9. Fertleman, C. R., Baker, M. D., Parker, K. A., Moffatt, S., Elmslie, F. V., Abrahamsen, B., Ostman, J., Klugbauer, N., Wood, J. N., Gardiner, R. M., and Rees, M. (2006) *Neuron* **52,** 767–774
10. Cox, J. J., Reimann, F., Nicholas, A. K., Thornton, G., Roberts, E., Springell, K., Karbani, G., Jafri, H., Mannan, J., Raashid, Y., Al-Gazali, L., Hamamy, H., Valente, E. M., Gorman, S., Williams, R., McHale, D. P., Wood, J. N., Gribble, F. M., and Woods, C. G. (2006) *Nature* **444,** 894–898
11. Cestele, S., and Catterall, W. A. (2000) *Biochimie (Paris)* **82,** 883–892
12. Shon, K. J., Stocker, M., Terlau, H., Stuhmer, W., Jacobsen, R., Walker, C., Grilley, M., Watkins, M., Hillyard, D. R., Gray, W. R., and Olivera, B. M. (1998) *J. Biol. Chem.* **273,** 33–38
13. Safo, P., Rosenbaum, T., Shcherbatko, A., Choi, D. Y., Han, E., Toledo-Aral, J. J., Olivera, B. M., Brehm, P., and Mandel, G. (2000) *J. Neurosci.* **20,** 76–80
14. Nielsen, K. J., Watson, M., Adams, D. J., Hammarstrom, A. K., Gage, P. W., Hill, J. M., Craik, D. J., Thomas, L., Adams, D., Alewood, P. F., and Lewis, R. J. (2002) *J. Biol. Chem.* **277,** 27247–27255
15. Lewis, R. J., Schroeder, C. I., Ekberg, J., Nielsen, K. J., Loughnan, M., Thomas, L., Adams, D. A., Drinkwater, R., Adams, D. J., and Alewood, P. F. (2007) *Mol. Pharmacol.* **71,** 676–685
16. West, P. J., Bulaj, G., Garrett, J. E., Olivera, B. M., and Yoshikami, D. (2002) *Biochemistry* **41,** 15388–15393
17. Keizer, D. W., West, P. J., Lee, E. F., Yoshikami, D., Olivera, B. M., Bulaj, G., and Norton, R. S. (2003)
18. Bulaj, G., West, P. J., Garrett, J. E., Marsh, M., Zhang, M.-M., Norton, R. S., Smith, B. J., Yoshikami, D., and Olivera, B. M. (2005) *Biochemistry* **44,** 7259–7265
19. Wang, C. Z., Zhang, H., Jiang, H., Lu, W., Zhao, Z. Q., and Chi, C. W. (2006) *Toxicon.* **47,** 122–132
20. Zhang, M. M., Green, B. R., Catlin, P., Fiedler, B., Azam, L., Chadwick, A., Terlau, H., McArthur, J. R., French, R. J., Gulyas, J., Rivier, J. E., Smith, B. J., Norton, R. S., Oliviera, B. M., Yoshikami, D., and Bulaj, G. (2007) *J. Biol. Chem.* **282,** 30699–30706
21. Zhang, M.-M., Fiedler, B., Green, B. R., Catlin, P., Watkins, M., Garrett, J. E., Smith, B. J., Yoshikami, D., Olivera, B. M., and Bulaj, G. (2006) *Biochemistry* **45,** 3731–3840
22. Chahine, M., Chen, L.-Q., Fotouhi, N., Walsky, R., Fry, D., Santarelli, V., Horn, R., and Kallen, R. G. (1995) *Receptors Channels* **3,** 161–174
23. Chang, G., Guida, W. C., and Still, W. C. (1989) *J. Am. Chem. Soc.* **111,** 4379–4386
24. Shon, K. J., Olivera, B. M., Watkins, M., Jacobsen, R. B., Gray, W. R., Floersca, C. Z., Cruz, L. J., Hillyard, D. R., Brink, A., Terlau, H., and Yoshikami, D. (1998) *J. Neurosci.* **18,** 4473–4481
25. Wakamatsu, K., Kohda, D., Hatanaka, H., Lancelin, J.-M., Ishida, Y., Oya, M., Nakamura, H., Inagaki, F., and Sato, K. (1992) *Biochemistry* **31,** 12577–12584
26. Lancelin, J.-M., Kohda, D., Tate, T., Yanagawa, Y., Abe, T., Satake, M., and Inagaki, F. (1991) *Biochemistry* **30,** 6908–6916
27. Hill, J. M., Alewood, P. F., and Craik, D. J. (1996) *Biochemistry* **35,** 8824–8835
28. Schnölzer, M., Alewood, P. F., Jones, A., Alewood, D., and Kent, S. B. H. (1992) *Int. J. Pept. Protein Res.* **40,** 180–193
29. Nielsen, K. J., Adams, D., Thomas, L., Bond, T., Alewood, P. F., Craik, D. J., and Lewis, R. J. (1999) *J. Mol. Biol.* **289,** 1405–1421
30. Moffatt, F., Senkans, P., and Ricketts, D. (2000) *J. Chromatogr. A.* **891,** 235–242
31. Daly, N. L., Ekberg, J. A., Thomas, L., Adams, D. J., Lewis, R. J., and Craik, D. J. (2004) *J. Biol. Chem.* **279,** 25774–25782
32. Piotto, M., Saudek, V., and Sklenar, V. (1992) *J. Biomol. NMR* **2,** 661–665
33. Wishart, D. S., Bigam, C. G., Holm, A., Hodges, R. S., and Sykes, B. D. (1995) *J. Biomol. NMR* **5,** 67–81
34. Goddard, T. D., and Kneller, D. G. (2004) *SPARKY 3*, University of California, San Francisco, CA
35. Guntert, P., Mumenthaler, C., and Wüthrich, K. (1997) *J. Mol. Biol.* **273,** 283–298
36. Brünger, A. T., Adams, P. D., and Rice, L. M. (1997) *Structure* **5,** 325–336
37. Rosengren, K. J., Daly, N. L., Plan, M. R., Waine, C., and Craik, D. J. (2003) *J. Biol. Chem.* **278,** 8606–8616
38. Cruz, L. J., Gray, W. R., Olivera, B. M., Zeikus, R. D., Kerr, L., Yoshikami, D., and Moczydlowski, E. (1985) *J. Biol. Chem.* **260,** 9280–9288
39. Nakamura, M., Niwa, Y., Ishida, Y., Kohno, T., Sato, K., Oba, Y., and Nakamura, H. (2001) *FEBS Lett.* **503,** 107–110
40. Becker, S., Prusak-Sochaczewski, E., Zamponi, G., Beck-Sickinger, A. G., Gordon, R. D., and French, R. J. (1992) *Biochemistry* **31,** 8229–8238
41. Sato, K., Ishida, Y., Wakamatsu, K., Kato, R., Honda, H., Ohizumi, Y., Nakamura, H., Ohya, M., Lancelin, J.-M., Kohda, D., and Inagaki, F. (1991) *J. Biol. Chem.* **266,** 16989–16991
42. Ott, K.-H., Becker, S., Gordon, R. D., and Ruterjans, H. (1991) *FEBS Lett.* **278,** 160–166